Can in situ measurements of mantle electrical conductivity be used to infer properties of partial melts?

Stephen K. Park
Institute of Geophysics and Planetary Physics, University of California, Riverside, California, USA

Mihai N. Ducea
Department of Geological Sciences, University of Arizona, Tucson, Arizona, USA

Received 27 March 2002; revised 3 February 2003; accepted 25 February 2003; published 24 May 2003.

[1] Constraints on bulk conductivity from magnetotelluric measurements and petrological analyses of late Quaternary peridotite xenoliths from the southern Sierra Nevada allow evaluation of models commonly used to relate electrical conductivity to the physical and chemical state of the upper mantle. In these models, two conductive melts (basalt and sulfide) are embedded in a resistive matrix. Bounds on the amount of sulfide (0.06–0.4%) and the bulk conductivity (0.03–0.1 S/m) place constraints on the degree of interconnection between the melts. Because the sulfide melt is very conductive, even a small fraction of well-connected melt results in a bulk conductivity larger than 0.1 S/m. Similarly, completely disconnected melts result in bulk conductivities much less than 0.03 S/m. The only models which matched both the bulk conductivity and sulfide bounds consisted of a small fraction (<1%) interconnected basalt melt with a discontinuous sulfide phase. Such a texture is observed in laboratory experiments with much larger sulfide melt fractions, but has not been reported for small melt fractions. A variant of the Hashin-Shtrikman model and a hybrid model consisting of cascaded Hashin-Shtrikman calculations were successful in matching the magnetotelluric and petrologic constraints. With a model that appropriately simulates the melt interconnectivity, we suggest that electrical conductivity may be used to infer in situ melt properties in the mantle. *INDEX TERMS:* 3914 Mineral Physics: Electrical properties; 8145 Tectonophysics: Physics of magma and magma bodies; 8434 Volcanology: Magma migration; *KEYWORDS:* mantle conductivity, Sierra Nevada, sulfide melt

Citation: Park, S. K., and M. N. Ducea, Can in situ measurements of mantle electrical conductivity be used to infer properties of partial melts?, *J. Geophys. Res.*, *108*(B5), 2270, doi:10.1029/2002JB001899, 2003.

1. Introduction

[2] Magnetotelluric (MT) studies are designed to provide a cross section and/or map of the variations of electrical conductivity within the crust and mantle [*Vozoff*, 1991]. Then, this distribution of conductivity is interpreted in its geologic context. Because the causes of electrical conductivity in the earth are many, some outside constraints are needed in order for the interpretation to be useful. A conductivity of 0.1 S/m (or alternatively, a resistivity of 10 ohm m) may be due to ions in groundwater in the shallowest 100 m, fractions of a percent of brine at depths of 10–20 km, or partial melt in the mantle at 40–70 km. Electrical conductivities of greater than 0.01 S/m in the lithosphere result from inclusion of a small fraction of a very conductive, interconnected phase, whether that phase is brine, partial melt, graphite, or metallic minerals. Interpretations of MT data often involve quantitative estimates of this small fraction using models of how that phase is connected [e.g., *Waff*, 1974; *Mareschal et al.*, 1995]. The models almost always involve a mix of two phases, a very conductive minor volume fraction and a resistive major volume fraction.

[3] *Ducea and Park* [2000] report mantle xenoliths from the Sierra Nevada that contained metallic sulfide grains and remnants of silicate melt along grain boundaries. They argue that the mantle contains both silicate and sulfide melts, based on the pressure and temperatures inferred from the xenoliths. The mantle thus has two conducting phases within a resistive matrix, a situation for which only a few models are applicable. *Ducea and Park* [2000] present a model wherein an equivalent melt created from the silicate and sulfide melts is embedded in a solid matrix and then conclude that the sulfide melt cannot form an interconnected phase. However, this result is not based on any accepted models that predict bulk conductivity from constituents.

[4] Here, we extend *Ducea and Park*'s [2000] work by showing that several accepted models matching the mineralogical, bulk conductivity, pressure, and temperature constraints also predict that the sulfide melt cannot be interconnected. We show that this prediction from models of the MT-derived conductivity is consistent with experi-

0148-0227/03/2002JB001899$09.00

Table 1. Constraints on the Upper Mantle

Property	Value
Pressure	1.3–2.3 GPa
Temperature	1180–1220°C
Sulfide content	<0.4%
Basalt melt	<2%

mental data on sulfide melts in mantle rocks. Finally, we conclude that MT data can be used to infer the connectivity of melts if xenolith data are available to constrain the mantle composition.

2. Constraints on Upper Mantle Conditions Beneath the Sierra Nevada

[5] All of the models examined here must satisfy constraints from MT and xenolith data; namely, they must yield a bulk conductivity of 0.03–0.1 S/m for partially melted mantle rocks containing metallic sulfide at a temperature of ~1200°C and a pressure of <1.8 GPa (Table 1). Sensitivity analyses of MT soundings in the southern Sierra Nevada show that conductivities at depths of 40–70 km that are larger than 0.1 S/m or smaller than 0.03 S/m produce unacceptably large misfits to the data [*Park et al.*, 1996]. Because Moho is only ~35 km deep beneath the southern Sierra Nevada [*Wernicke et al.*, 1996; *Ruppert et al.*, 1998], these conductivities must lie in the mantle. This region must contain partial melt; high electrical conductivities [*Park et al.*, 1996] and low seismic velocities [*Jones et al.*, 1994] are found here. The composition of the modern mantle must be peridotitic because *Ducea and Saleeby* [1996] document Quaternary peridotitic xenoliths from the eastern Sierra Nevada that equilibrated at temperatures of 1180–1220°C and pressures of 1.2–1.8 GPa (Figure 1). Additionally, *Moore and Dodge* [1980] and *Dodge and Moore* [1981] report late Quaternary xenolith-bearing basalts in the eastern Sierra Nevada region as young as a few thousand years old. Thus several lines of evidence indicate partial melt beneath the southern Sierra Nevada. This region of partial melt is inferred to be asthenosphere replacing lithosphere that delaminated since the Pliocene [*Ducea and Saleeby*, 1998; *Lee et al.*, 2000, 2001]. This delamination led to dramatic changes in the sub-Sierran mantle, as indicated by comparison of Miocene, Pliocene, and late Quaternary xenoliths [*Ducea and Saleeby*, 1998] and of the Miocene and Pliocene basalts [*Farmer et al.*, 2002]. Because the MT method looks only at the modern conditions, we have limited our discussion to the late Quaternary xenoliths.

[6] While an early model attributes the bulk conductivity solely to 2–5% basalt melt [*Park et al.*, 1996], *Ducea and Park* [2000] outline objections to this high a volume of partial melt. First, the basalt flows observed at the surface are volumetrically too minor to account for this much partial melt. Given the amount of late Cenozoic extension in the region [*Snow and Wernicke*, 1998], it is unlikely that the crust acted as a cap to prevent partial melt escaping to the surface. Second, seismic data shows no evidence of basalt underplating [*Ruppert et al.*, 1998]. Third, petrological modeling using MELTS [*Ghiorso and Sack*, 1995] with the observed xenolith compositions indicate only 1–2% partial melting (Figure 2). Such a small amount of melt cannot account for the observed mantle conductivities, leading *Ducea and Park* [2000] to look for other causes and to discover 0.06–0.4% sulfides in the Quaternary xenoliths. A small amount of sulfide could reduce the volume of basalt needed to less than 1% [*Ducea and Park*, 2000]. The monosulfide series begins melting at temperatures above 1150°C for a pressure of 1 GPa and 1200°C at a pressure of 2.0 GPa [*Lorand and*

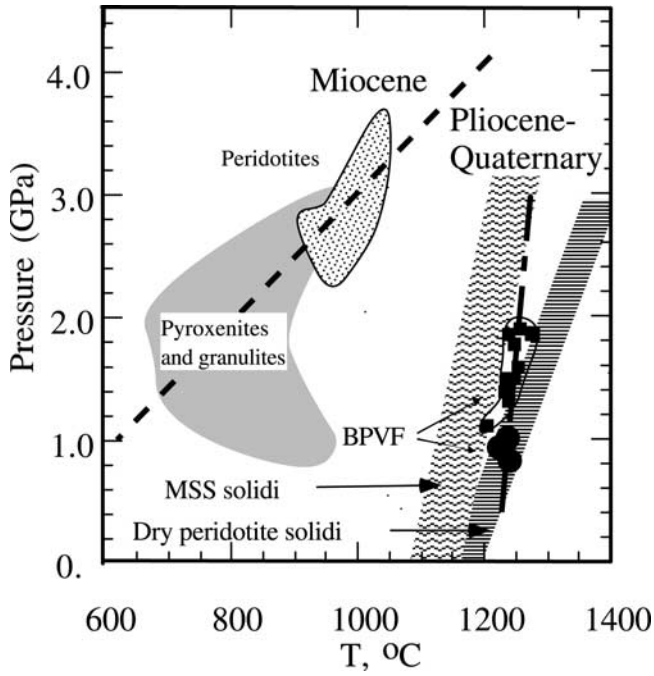

Figure 1. Equilibration pressures and temperatures for xenoliths (modified from *Ducea and Saleeby* [1996]). Spinel-bearing xenoliths (squares) and spinel- and plagioclase-bearing xenoliths (filled circles) from the Big Pine Volcanic Field (BPVF) are shown. Note how Pliocene and Quaternary xenoliths exhibit much higher temperatures, which fall above the MSS solidus range (MSS solidi) and extend into the peridotite solidi.

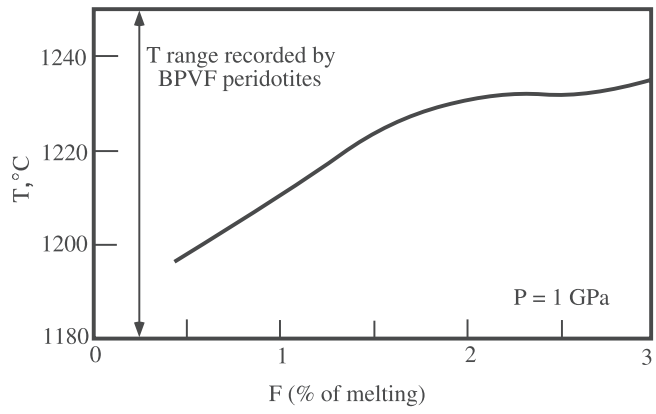

Figure 2. Melt fractions (F) as a function of temperature for a peridotite (spinel lherzolite) using the MELTS algorithm [*Ghiorso and Sack*, 1995]. The calculation was performed at a pressure of 1 GPa assuming batch melting.

Conquere, 1983], so its coexistence with basalt melt (which melts at higher temperatures) is expected (Figure 1).

3. Coexistence of Basalt and Sulfide Melts

[7] Sulfides are clearly found in the xenoliths now, but do they indicate a separate melt phase in the mantle? They could be remnants of a separate melt or could result from exsolution from the basalt melt during ascent. If a separate interconnected sulfide melt exists, then its effect on the bulk conductivity could be profound. If the sulfur is simply dissolved in the basalt melt, then the sulfide contribution to bulk conductivity should be negligible. *Ducea and Park* [2000] assumed that the sulfides formed a distinct phase in the mantle because the sulfide grains were seen in the xenoliths; here, we examine this assumption and show that the sulfides likely formed from a separate melt.

[8] Sulfides in mantle rocks have only recently been intensely studied because they affect the behavior of the commonly used Os isotopic system [*Pearson et al.*, 2002]. They might also offer clues on the early Earth mechanisms of accretion [e.g., *Alard et al.*, 2000]. The composition of mantle sulfides falls within the framework of a monosulfide solution of Fe, Cu and Ni (MSS); MSS exsolves at low temperatures during cooling of the mantle samples into pyrrhotite, chalcopyrite, and pentlandite. While sulfide content is hard to estimate by standard techniques such as point counting due to low concentrations, the average sulfide content in peridotites does not exceed 0.03–0.1% by volume [*Lorand*, 1990]. Western United States mantle peridotites have generally higher amounts of sulfides (∼0.08%) compared to European peridotite massifs [*Lorand*, 1989], mantle xenoliths from central and eastern Europe [*Lorand*, 1990; *Szabo and Bodnar*, 1995], Australia [*Handler and Bennett*, 1999], and China [*Guo et al.*, 1999]. Bulk rock measurements indicate that sulfur concentrations in continental upper mantle assemblages are about 200–350 ppm [*Lorand*, 1990]. Modal analyses of thirty xenoliths from the eastern Sierra Nevada conducted for this study indicate sulfide concentrations of 0.06–0.4% by volume, with and average of 0.09% by volume in peridotites (equivalent of S ∼ 300 ppm sulfur concentration), within the range of previously estimated sulfide concentrations in the shallow mantle beneath the western United States [*Dromgoole and Pasteris*, 1987; *Wilson et al.*, 1996] and also within the range, but at the higher end of sulfur concentrations worldwide. We observe no correlation between textural types of peridotites or fertility of peridotites (i.e., modal concentration of clinopyroxene) and the amount of sulfides present in the Sierran peridotites.

[9] Studies of MSS mantle sulfides indicate that most likely they represent the quenched products of sulfide melts. MSS melt slightly below 1100°C at 1 GPa [*Ryzenkho and Kennedy*, 1973]; it is therefore expected that if sulfides were present within a hot shallow mantle assemblage such as the one preserved in xenoliths from the eastern Sierra Nevada-western Basin and Range, they will be molten (Figure 1). In comparison, a cold geotherm characteristic for Archean cratons will not cross the MSS solidus within the upper 200 km. Sulfides are expected to be molten throughout much of the shallow mantle of the Basin and Range province, given the high equilibration temperatures of spinel peridotites (see *Smith* [2000] for a regional review of peridotite thermometry).

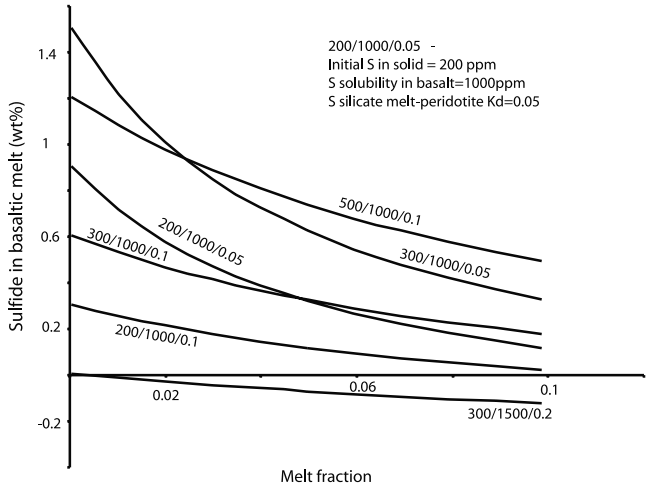

Figure 3. Estimated fraction of immiscible sulfide melt assuming batch melting, sulfur-silicate melt partition coefficients of 0.05–0.1, initial solid mantle sulfur concentrations of 200–400 ppm, and S solubilities of 1000–1500 ppm [see also *Keays*, 1995]. *Kd*, the sulfur partition coefficient, is the ratio of the sulfur concentration in the residual solid mantle to the sulfur concentration in the melt. While this partition coefficient is not well established (see summary at http://www.EarthRef.org/GERM), it is generally accepted that sulfur is an incompatible element during mantle melting [e.g., *Lorand*, 1990]. We use *Kd* = 0.05 and 0.1 for modeling here.

[10] The sulfide melts could have formed in one of three ways: (1) independently of any other melt as immiscible fluids due to the overall heating of the extending Basin and Range; (2) as immiscible liquids formed at sulfur saturation in silicate melts [e.g., *Dromgoole and Pasteris*, 1987]; or (3) in conjunction with a CO_2 gas-rich phase [*Shaw*, 1997]. The second explanation is thought to be the most common process responsible for the generation of sulfides with textural appearance of former melts, which is commonly observed in upper mantle xenoliths.

[11] A plausible mechanism capable of generating new sulfide in a hot, asthenospheric-like shallow mantle like the one beneath the eastern Sierra Nevada region is liquid immiscibility. Silicate liquids either generated in situ or traveling from greater depths to the mantle represented by the xenoliths can exsolve sulfide melts. The silicate-sulfide liquid immiscibility has been well documented at both low and high pressures in basalt systems [*Naldrett*, 1989]. If the amount of sulfur present in the magma exceeds the solubility, it will form a second immiscible liquid phase whose composition is of a typical MSS [*Fleet and Pan*, 1994]. The solubility of sulfur in basalt liquids at 1.0–1.5 GPa is about 1000–15000 ppm [*Mavrogenes and O'Neill*, 1999]. Immiscible sulfide melt fractions of 0.2–1.4 wt % are predicted to coexist with basalt melts at 1.0–1.5 GPa and low (<5%) melt fractions (Figure 3). The ratio of sulfide to silicate melt depends on the silicate melt fraction: the lower the silicate melt fraction, the higher the sulfide/silicate ratio. If the presence of sulfide melt can increase the electrical conduc-

tivity of partially molten mantle, that effect is expected only for lower silicate melt fractions.

[12] Silicate melts typically escape their mantle source regions, even at low melt fraction because of their mobility. In contrast, it is commonly assumed that sulfide melts remain in the mantle [e.g., *Dromgoole and Pasteris*, 1987] due to their high density (3.8–4 g/cm^3) for molten MSS [*Kaiura and Toguri*, 1979]. Clearly, this must be true to some extent; the sulfides seen in peridotite xenoliths from the eastern Sierra Nevada show textural evidence that they were once molten and quenched within the peridotite framework. The corresponding silicate melt is rarely seen as glass inclusions. However, the dynamic details of this complex multiphase solid-melt system are unknown and we suspect that some sulfide mobility at meter to kilometer scale as melt is very plausible.

[13] Immiscible sulfide melts likely formed in the shallow sub-Sierran mantle and that those melts have likely remained there since formation. However, the connectivity within and between the silicate and sulfide melts affects their influence on bulk conductivity. *Holzheid et al.* [2000] observe dihedral angles between sulfide and silicate melts of greater than 60° and of 60–125° between sulfide melts and olivine at pressures of 1.5 GPa and temperatures of 1370–1410°C, but these experiments were done with much larger percentages (~35%) of sulfide melt. Dihedral angles greater than 60° imply disconnected melts, and sulfide melts are observed to form pockets on the surfaces of the olivine matrix, while the basalt melt forms an interconnected phase. However, *Gaetani and Grove* [1999] show that dihedral angles can be reduced to slightly less than 60° by dissolving up to 10 wt % oxygen in sulfide melt at 0.1 KPa pressure and a temperature of 1350°C. Reduction of the dihedral angle could permit sulfide melt interconnection, but *Minarek et al.* [1996] shows that pressure increases the angle to as high as 90° for the same temperatures and dissolved oxygen. Because *Gaetani and Grove* [1999] were only able to reduce the dihedral angle to slightly less than 60° at 0.1 KPa, we suggest that our sulfide melts at 1 GPa will not form an interconnected network.

4. Component Conductivities

[14] We wish to compute bulk conductivities from mixes of sulfide melt, basalt melt, and peridotite matrix, but need the conductivities of the components to do this. Conductivities of the basalt melt and peridotite matrix can generally be estimated from previous laboratory experiments. The largest uncertainty comes from the conductivity of the sulfide melt, which has never been measured. *Duba et al.* [1994] have measurements of 10^3–10^5 S/m for solid sulfide; *Olhoeft* [1981] has similar values for chalcocite, chalcopyrite, pyrite, and pyrrhotite. While we anticipate that the melt is at least as conductive as the solid because of the greater ionic mobility in a fluid, we choose a conservative value of 10^4 S/m for the melt.

[15] Conductivities of the basalt melt can vary with composition, temperature, and oxygen fugacity. *Roberts and Tyburczy* [1999] show that the conductivity can vary by as much as an order of magnitude, from 1 S/m at 1150°C to 10 S/m at 1250°C. Direct measurement of melt conductivity is difficult and rarely done. Instead, measurements of bulk conductivity on partially melted samples are made and then models such as the ones discussed here are used to determine melt conductivity. In an alternate approach, *Roberts and Tyburczy* [1999] use an equilibrium melt fraction program (MELTS) by *Ghiorso and Sack* [1995] to predict melt fraction and then estimate melt conductivity from this predicted fraction and measurements of bulk conductivity using an upper bound model from *Hashin and Shtrikman* [1962]. (The Hashin-Shtrikman (HS) upper bound model is presented in the next section.) They compute values of 0.65–0.98 S/m for temperatures comparable to ours, but conclude that their values were lower than true values by approximately a factor of 3 because of partial melt disconnection. *Park et al.* [1996] and *Ducea and Park* [2000] use *Shankland and Waff*'s [1977] equation for basalt melt conductivity:

$$\sigma_{\mathrm{melt}} = \sigma_0 \exp(-E_a/kT), \tag{1}$$

where E_a = 1.15 eV, σ_0 = 18,400 S/m, k is the Boltzmann constant, and T is absolute temperature in K. Equation (1) predicts values of 1.55 S/m at 1150°C to 2.86 S/m at 1250°C, which are consistent with those from *Roberts and Tyburczy* [1999]. Although *Tyburczy and Waff* [1983] determined values of E_a = 1.53 eV and σ_0 = 215,000 S/m for tholeiitic melt, equation (1) with these parameters predicts values of 0.80–1.85 S/m for melt between 1150–1250°C. Because Shankland and Waff's parameters are closer to what Roberts and Tyburczy's more recent study predicts, we use their values in our models (Table 2). Use of a higher conductivity for the basalt melt fraction will decrease the melt fractions needed to produce a given bulk conductivity, so the melt fractions we calculate will be minimum values. In all measurements, the basalt melt conductivity varies by a factor of ~2 over the temperature range in Table 1.

Table 2. Thermodynamic Parameters for Matrix Minerals

Mineral	σ_0, S/m	E_a or E_{a1}, eV	E_{a2}, eV
ol		1.60	4.25
opx	5248	1.80	
cpx	1778	1.87	

[16] We estimate the conductivity of the solid matrix from its composition, pressure, and temperature. *Ducea and Park* [2000] use solid olivine as a matrix, following the observations that lherzolite conductivity can be modeled with that of olivine [*Constable and Duba*, 1990]. However, *Xu et al.* [2000] show that both orthopyroxene (opx) and clinopyroxene (cpx) are more conductive than olivine at depths in excess of 200 km. They calculate the bulk conductivity for a pyrolite (60% olivine, 25% opx, and 15% cpx) using the HS upper bound model, and conclude that the conductivities match the observations well. We will also use the HS upper bound for computing the bulk conductivity of the matrix, but alter the percentages of minerals based on analyses of late Quaternary peridotite xenoliths (Table 3). Note that these analyses are very similar to that of a standard pyrolite model (Table 3) and we assume that metasomatism of the modern asthenosphere is not a factor here. At 1 GPa and temperatures of 1050–1200°C with the pyrolite compo-

Table 3. Xenolith Compositions[a]

	Harzburgite	Lherzolite	Harzburgite	Lherzolite	Peridotite	Pyrolite
SiO_2	40.94	44.78	41.13	44.30	45.00	46.31
Na_2O	0.61	0.56	0.77	0.16	0.49	0.63
MgO	36.78	35.38	33.92	40.50	36.40	38.50
Al_2O_3	4.49	4.06	4.45	2.74	3.20	4.61
P_2O_5	0.01	0.01	0.02	0.05	0.01	0.00
K_2O	0.01	0.01	0.08	0.03	0.07	0.00
CaO	2.69	3.30	5.24	2.12	4.40	3.72
TiO_2	0.31	0.21	0.93	0.04	0.25	0.21
MnO	0.16	0.16	0.18	0.15	0.12	0.14
FeO(total)	13.12	10.64	12.94	9.25	9.50	5.82
Total	99.12	99.11	96.66	9.34	99.44	99.94

[a]Compositions in wt %.

sition in Table 3, MELTS [*Ghiorso and Sack*, 1995] predicts that the matrix consists of 54–55% olivine, 26–27% opx, 16–17% cpx, and 1.5% spinel. For our calculation, we use a model of 55% olivine, 27% opx, and 18% cpx under the assumption that the minor fraction of spinel contributes negligibly.

[17] The conductivity of the olivine fraction is calculated using the SO2 model [*Constable et al.*, 1992]:

$$\sigma_{\text{olivine}} = 10^{2.4}\exp(-E_{a1}/kT) + 10^{9.17}\exp(-E_{a2}/kT), \quad (2)$$

where E_{a1} and E_{a2} are given in Table 2. The temperature-dependent conductivity of opx and cpx is modeled using

$$\sigma_{\text{solid}} = \sigma_0\exp[-E_a/kT], \quad (3)$$

with parameters (Table 2) from *Xu et al.* [2000]. Calculations of the effective conductivity of the pyrolite (HS+) shows that this matrix is approximately 1.6 times more conductive than olivine (Figure 4) and matches the lherzolite measurements of *Constable and Duba* [1990]. Given that matrix conductivities of 0.0005–0.003 S/m are so much lower than conductivities of either the basalt or sulfide melts, we conclude that uncertainties in the matrix conductivity will have a negligible effect on the bulk conductivity.

5. Models and Melt Connectivity

[18] We next consider how to combine the component conductivities into a bulk value for the mantle. Many models have been used to predict laboratory measurements of bulk conductivity from rock composition and state; we consider only the most common ones here that can be generalized to multiple phases and include an equivalent medium model that we have derived. For the purposes of calculations, we will use fractions of sulfide from 0.01 to 10% and fractions of basalt melt from 0.01 to 10%. Below 0.01%, it is unclear whether melts will form an interconnected network. Above 10%, most models predict too high a bulk conductivity.

5.1. Series and Parallel Models

[19] Series and parallel models [e.g., *Waff*, 1974; *Roberts and Tyburczy*, 1999] are the simplest models used and formulae for these can be found in introductory physics texts [e.g., *Halliday et al.*, 1997]. If N different phases with volume fraction f_i and conductivity σ_i are combined in series, then the effective conductivity (σ_{eff}) of the rock is

$$\sigma_{\text{eff}} = 1\Big/\sum_{i=1}^{n}\frac{f_i}{\sigma_i}. \quad (4)$$

The parallel model assumes the phases are connected in parallel:

$$\sigma_{\text{eff}} = \sum_{i=1}^{n} f_i\sigma_i. \quad (5)$$

The parallel model might seem more appropriate for an interconnected melt fraction within a matrix because both phases can conduct current in parallel, but the rock may contain paths in which current must flow across the matrix between two sections of melt (i.e., series connection). Thus a geometric mean of equations (4) and (5) is often used to simulate this mix of series and parallel connections [*Madden*, 1976].

[20] The series model of our system underestimates the bulk conductivity, while the parallel model overestimates it

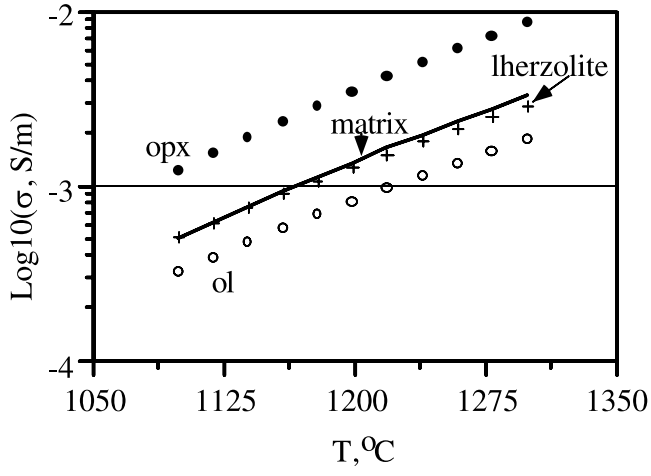

Figure 4. Matrix conductivity (pyrolite line) predicted from the HS upper bound using parameters from *Xu et al.* [2000]. Symbols show conductivities of components orthopyroxene (opx, solid circles), olivine (ol, open circles), and lherzolite (crosses). Note that the pyrolite model is more conductive than olivine and matches the lherzolite well.

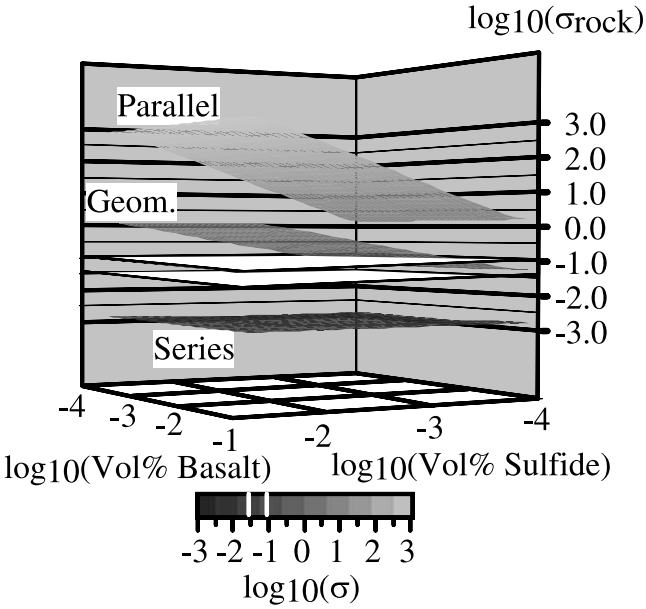

Figure 5. Series, parallel, and geometric mean models for basalt, sulfide, and matrix mix at a pressure of 2.3 GPa and temperature of 1200°C. Only the geometric mean passes through the through the region with bulk conductivity between 0.03 and 0.1 S/m (shown by white surfaces). The range of permissible values of bulk conductivity is shown by the white lines on the scale.

(Figure 5). The bulk conductivity in the series model, from 0.0013 to 0.0016 S/m, is dominated by the resistive matrix. The bulk conductivity in the parallel model, from 1 to 1000 S/m, is dominated by the highly conductive sulfide melt. In both cases, the basalt melt contributes little to the bulk response. The geometric mean results in values that fall within the permissible range of bulk conductivities, however (Figure 5). While this mean is viable model, it requires 0.01–0.07% sulfide melt and is relatively insensitive to the amount of basalt melt (Figure 6). The geometric mean is still dominated by its most conductive phase, the sulfide melt. This range of sulfide melt is also low compared to the range of sulfides observed (Table 1).

5.2. Hashin-Shtrikman Bounds

[21] One of the most widely used models is that of *Hashin and Shtrikman* [1962]. The HS model is one of the few calculations that explicitly includes multiple phases and is based on absolute upper and lower bounds on the electrostatic energy of the composite medium. The lower bound of effective conductivity of a system consisting of phases $\sigma_1 < \sigma_2 < \sigma_3 \ldots < \sigma_n$ with volume fractions $f_1, f_2, f_3, .., f_n$ is

$$\sigma_{\text{eff,HS}-} = \sigma_{\min} + \frac{A_{\min}}{1 - A_{\min}/(3\sigma_{\min})}, \tag{6}$$

where $\sigma_{\min}$ ($=\sigma_1$) is the minimum conductivity in σ_i and [*Hashin and Shtrikman*, 1962]

$$A_{\min} = \sum_{i=2}^{n} \frac{f_i}{\left[(\sigma_i - \sigma_{\min})^{-1} + (3\sigma_{\min})^{-1}\right]}. \tag{7}$$

The upper bound is given by

$$\sigma_{\text{eff,HS}+} = \sigma_{\max} + \frac{A_{\max}}{1 - A_{\max}/(3\sigma_{\max})}, \tag{8}$$

where $\sigma_{\max}$ ($=\sigma_n$) is the maximum conductivity in σ_i and

$$A_{\max} = \sum_{i=1}^{n-1} \frac{f_i}{\left[(\sigma_i - \sigma_{\max})^{-1} + (3\sigma_{\max})^{-1}\right]}. \tag{9}$$

Hashin and Shtrikman [1962] showed that for two phases, these equations reduce to those for a composite sphere with an outer shell of $\sigma_{\min}$ for the lower bound and an outer shell of $\sigma_{\max}$ for the upper bound. In both cases, the outer shell is effectively the interconnected phase and the inner one is disconnected. For a binary system consisting of melt and matrix, the upper bound would represent an interconnected melt phase surrounding matrix grains and the lower bound would represent isolated melt pockets surrounded by matrix grains.

[22] HS upper and lower bounds overestimate or underestimate the bulk conductivity, respectively. The upper bound (8) predicts a range of 0.631–631 S/m (Figure 7), while the lower bound (6) predicts a range of 0.00079–0.0013 S/m. Our observed values of 0.03–0.1 S/m do fall within these bounds, but the bounds have little utility because estimates of melt content would be much too high or low. The HS upper bound is uniformly too

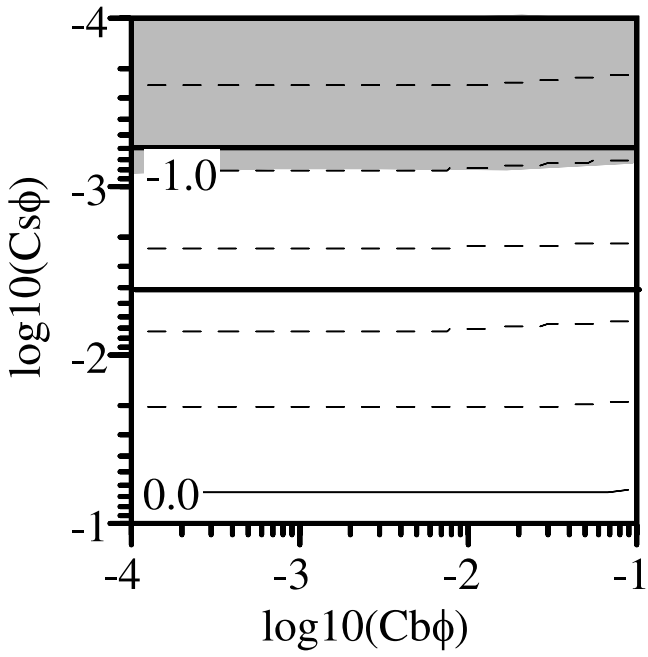

Figure 6. The $\log_{10}$(bulk conductivity) plotted versus $\log_{10}$(basalt, $C_b\varphi$) and $\log_{10}$(sulfide, $C_s\varphi$) melt fractions for geometric mean model. Fractions are converted to percentages used in text by multiplying by 100. Shaded region shows range of permissible bulk conductivities, and horizontal lines show range of observed sulfide fractions. Note that bulk conductivity is almost independent of basalt fraction.

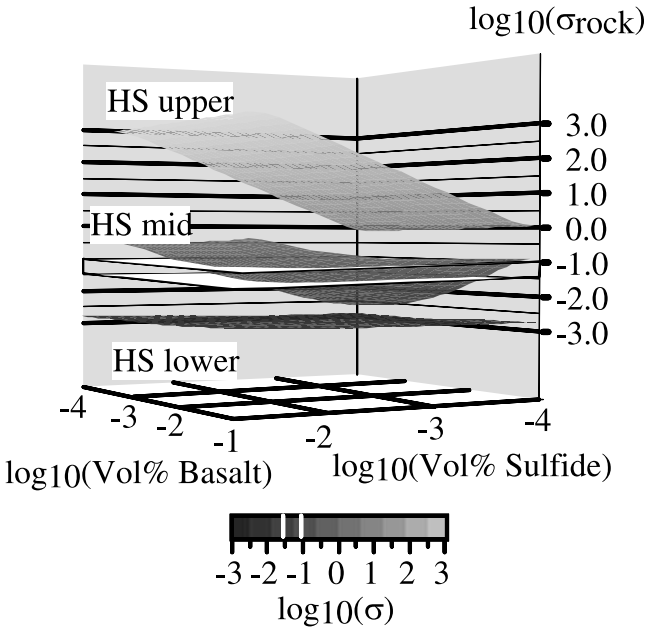

Figure 7. Hashin-Shtrikman bounds for the basalt, sulfide, and matrix mix at a pressure of 2.3 GPa and temperature of 1200°C. The upper bound has sulfide melt as the outer shell, and the lower bound has the matrix as the outer shell. The middle bound has the basalt as the outer shell and is the only one that passes through the region with bulk conductivity between 0.03 and 0.1 S/m (shown by white surfaces). The range of permissible values of bulk conductivity is shown by the white lines on the scale.

conductive because it permits the sulfide melt to form an interconnected phase. The HS lower bound is uniformly too resistive because it isolates melt pockets from each other by surrounding them with the resistive matrix.

[23] We also examine a model based on the Hashin-Shtrikman method that does not assume that the most conductive or most resistive phase is interconnected. Based on the fact that the upper and lower bounds are analogous to interconnected sulfide or matrix phases respectively, we calculate a Hashin-Shtrikman model with basalt melt as the interconnected phase:

$$\sigma_{eff,HSm} = \sigma_{basalt} + \frac{A_{mid}}{1 - A_{mid}/(3\sigma_{basalt})}, \qquad (10)$$

where

$$A_{mid} = \sum_{i'=1}^{n} \frac{f_i}{\left[(\sigma_i - \sigma_{basalt})^{-1} + (3\sigma_{basalt})^{-1}\right]}, \qquad (11)$$

where i' excludes the basalt phase. Note that there is no loss of validity in the use of the Hashin-Shtrikman formula for calculation of an effective conductivity; it just no longer provides absolute bounds. The model also specifies nothing about the distribution of the sulfide melt or matrix except that heterogeneities are small compared to the size of the averaging region [*Hashin and Shtrikman*, 1962]. This model predicts conductivities within the range of the Sierran observations (Figure 7) but requires ~0.8–6% basalt melt in order to also match the range of observed sulfide content (Figure 8). The lower end of this range satisfies the needs outlined by *Ducea and Park* [2000] for low basalt melt fractions.

5.3. Spherical Inclusion Models

[24] The HS models are exactly equivalent to layered spheres for two-phase media [*Hashin and Shtrikman*, 1962; *Waff*, 1974]. This equivalence led us to extend *Hashin and Shtrikman*'s [1962] derivation for the equivalent conductivity of a two-phase sphere to a three-phase sphere. Inclusion of additional layers to their model is conceptually trivial but analytic expressions for the effective conductivity become increasingly complicated. A key point is that a model of an equivalent medium created by embedding an infinite number of spheres with an infinite range of radii is valid only if the maximum radius is small compared to the distance at which the observations of potential are made. Grain sizes in the mantle at depths of 40–70 km are typically ~1 mm, so this assumption should be satisfied. Details of the derivation are provided in the Appendix; we just outline the steps here and then present the result. The goal is to find a homogeneous sphere with an equivalent conductivity, σ_{eff}, that perturbs a uniform electric field in the same manner as does the layered sphere (Figure 9). Then, the electrostatic energy of both spheres is equal. With σ_1 forming the core of the sphere and σ_3 forming the outermost shell,

$$\sigma_{eff} = \sigma_3 \left[\frac{2f_3S_3(\alpha+1) - (2\alpha-1)(3-2f_3)}{S_3(\alpha+1)(3-f_3) + f_3(1-2\alpha)}\right], \qquad (12)$$

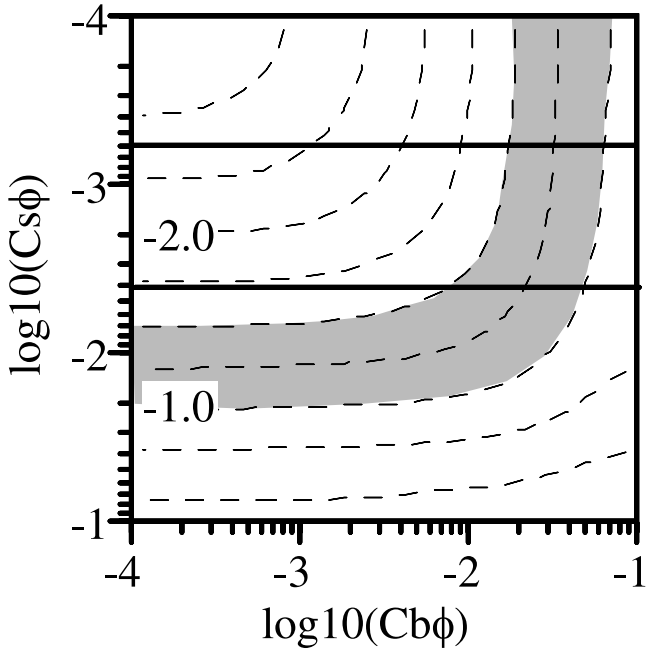

Figure 8. The $\log_{10}$(bulk conductivity) plotted versus $\log_{10}$(basalt, $C_b\varphi$) and $\log_{10}$(sulfide, $C_s\varphi$) melt fractions for HS middle bound. See caption of Figure 6 for explanation.

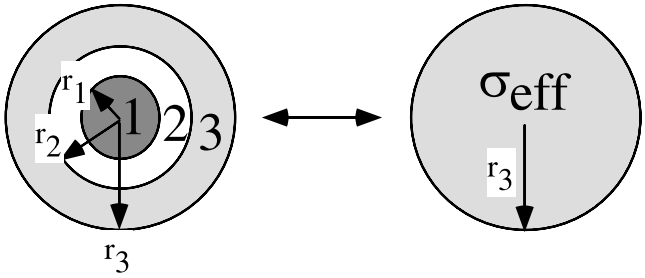

Figure 9. Composite and equivalent spheres. Inner shell has conductivity σ_1 and radius r_1, middle shell has conductivity σ_2 and extends to radius r_2, and the outer shell has conductivity σ_3 and outer radius r_3.

where $S_3 = \sigma_3/\sigma_2$, f_i is the volume fraction of the ith phase, and

$$\alpha = \frac{f_1(\sigma_2 - \sigma_1)}{(2\sigma_2 + \sigma_1)(f_1 + f_2)}. \quad (13)$$

An infinite number of equivalent spheres with an infinite range of radii are then used to fill the space, resulting in a homogeneous equivalent medium. Equations (12) and (13) reduce to *Waff*'s [1974] result for a sphere with 2 phases when $\sigma_1 = \sigma_2$. Note that only the phase in the outermost shell is explicitly interconnected.

[25] Six possible layered spherical models can be examined because of the combinations of three phases (sulfide melt, basalt melt, matrix). Both of the models with olivine as the interconnected phase (i.e., the outer shell) predict conductivities that are too low to match our constraints (Table 4). This is because, like the HS lower bound, the resistive matrix blocks current flow between the conductive fractions. Indeed, these models predict conductivities comparable to those of the HS lower bound. In contrast, both of the models with sulfide as the interconnected phase predict conductivities that are too high to match our constraints but are comparable to those of the HS upper bound or parallel model (Table 4 and Figure 10). The sulfide melt essentially shorts out current flow. The two remaining models have basalt melt as the interconnected phase, but produce very different results (Table 4).

[26] In the first model with basalt melt as the outer phase, the sulfide melt is in contact with the basalt and conductivities are indistinguishable from those where the sulfide is the outer phase and basalt is the middle shell (Table 4). One way to explain this result is that the sulfide melt forms intact shells around matrix cores and is locally interconnected. The complete connection between the outer basalt melt and middle sulfide melt results in a high effective conductivity for the interconnected melt phase. This model does not match the constraints from the MT data.

Table 4. Conductivity Ranges for Sphere Models

Shell				
Inner	Middle	Outer	log 10(min)	log 10(max)
Basalt	sulfide	matrix	−2.9	−2.6
Sulfide	basalt	matrix	−2.9	−2.6
Basalt	matrix	sulfide	−0.2	2.8
Matrix	basalt	sulfide	−0.2	2.8
Matrix	sulfide	basalt	−0.2	2.8
Sulfide	matrix	basalt	−2.8	−0.8

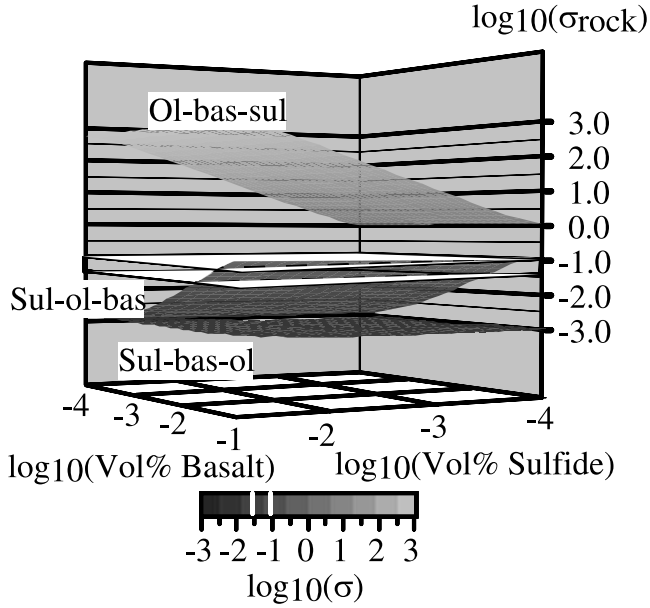

Figure 10. Three composite sphere models for a pressure of 2.3 GPa and temperature of 1200°C. The model with the olivine core and sulfide outer shell (ol-bas-sul) has the highest effective conductivities and resembles the HS upper bound from Figure 7. The model with the sulfide core and olivine outer shell (sul-bas-ol) resembles the HS lower bound. The model with the sulfide core and basalt outer shell (sul-ol-bas) passes through the region of our data.

[27] The second model has sulfide melt isolated from the silicate melt by a middle shell of matrix. This model predicts conductivity values between 0.00079 and 0.158 S/m, which span the observed range of 0.03–0.1 S/m (Table 4 and Figure 10). However, this model predicts conductivity values that are virtually identical to those from a binary system consisting of a basalt outer shell and matrix inner shell (results not shown here). The isolated sulfide melt has no effect on the bulk conductivity, and this model would require basalt melt percentages similar to those of *Park et al.* [1996]. A more complicated model with the sulfide melt forming a locally discontinuous phase as a middle shell is needed; such a model is not amenable to analytic expressions, however.

5.4. Hybrid Models

[28] Most of the models predict bulk conductivities that lie uniformly above or below the constrained range from MT observations and/or do not satisfy the constraints from the xenoliths. Only three models predict bulk conductivities within the desired range, and two of them (geometric mean and spherical inclusion model with interconnected basalt melt and disconnected sulfide melt) are marginal. The geometric mean model requires volume fractions of sulfides that are just barely within the range of observed values. The spherical inclusion model predicts that the sulfide must be isolated from the basalt melt; a requirement that contradicts

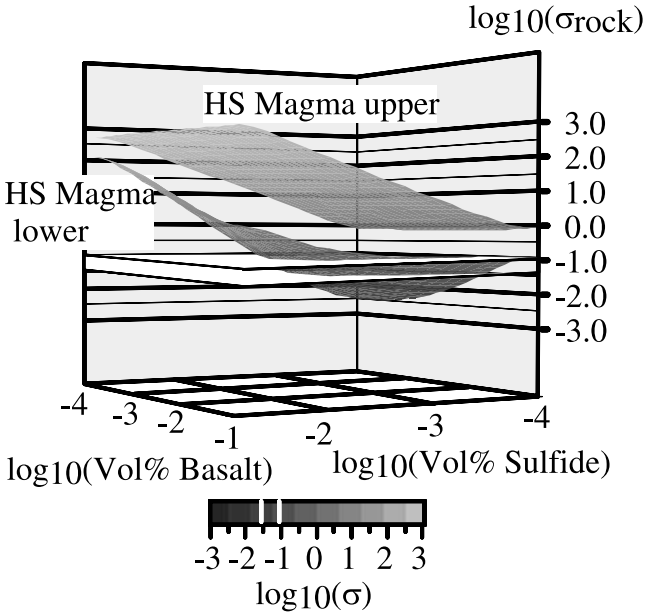

Figure 11. Hybrid models of an HS upper bound for the melt (HS magma upper) and lower bound (HS magma lower). In both cases, the HS upper bound was used to estimate the melt-matrix bulk conductivity. Calculations were done at $P = 2.3$ GPa and $T = 1200°C$. Note how only the HS lower magma bound passes through the region of permissible conductivities.

the observed textures [*Holzheid et al.*, 2000]. Only the HS middle bound satisfies both the observed bulk conductivities and sulfide fractions.

[29] *Ducea and Park* [2000] showed that a cascade application of the HS bounds can also be used to derive an analytic expression that satisfies the constraints in Table 1. In their model, the sulfide and basalt melts are first mixed using an HS lower bound (6) and then the effective melt is embedded in an isotropic, cubic block model [*Waff*, 1974]. We complement their calculations by using both the HS upper (8) and lower bounds (6) for the melt and then embedding this melt in a matrix using the HS upper bound (8). This approach results in analytic expressions for bulk conductivity, but only that with the HS lower bound for the melt predicts values that fall within the desired range (Figure 11). Because an interconnected fluid composed of a disconnected sulfide melt and an interconnected basalt melt in a solid matrix is identical to that of *Ducea and Park* [2000], a contour map of the bulk conductivity in Figure 11 is identical to their Figure 4 and is not shown here. Note that a model with an interconnected sulfide phase predicts bulk conductivities that are at least 10 times greater than observed; sulfide melts cannot act as interconnected conductors.

6. Discussion

[30] The modeling tests presented above have two goals. First, we seek a model that predicts a basalt melt fraction of less than ~1% for temperatures of 1180–1220°C, bulk conductivities of 0.03–0.1 S/m, and sulfide melt fractions of 0.06–0.4%. Second, we seek models that are consistent with laboratory observations of melt relationships (interconnected basalt melt and isolated sulfide melt pockets). All of the models tested that contain an interconnected sulfide melt predict bulk conductivities that are much larger than observed. Similarly, all models with completely isolated melt fractions predict bulk conductivities that are much lower than expected. Interconnected melt fractions are required to match the MT-derived constraints on bulk conductivity, but only the basalt melt can be interconnected.

[31] Models which satisfy the bulk conductivity and sulfide melt constraints include the geometric mean, spherical inclusion model with an outer shell of basalt melt, the HS middle bound, and the hybrid model used by *Ducea and Park* [2000]. These models have a discontinuous sulfide melt in contact with an interconnected basalt melt which is embedded in a resistive matrix. However, some of these models showed no sensitivity to one or the other of the melt fractions. The geometric mean model, while falling within the acceptable bounds, predicts that the basalt melt fraction has no effect on the bulk conductivity (Figure 6). The bulk conductivity is dominated by the fraction of sulfide melt in this model because it allows substantial fractions of connected sulfide melt. This behavior contradicts textural evidence [*Holzheid et al.*, 2000], and we suggest that the geometric mean should not be used for this situation.

[32] The spherical inclusion model predicts the opposite result that the sulfide melt has no effect on bulk conductivity because the sulfide is isolated from the basalt melt by shells of matrix. This again contradicts textural evidence from *Holzheid et al.* [2000] that the sulfide and basalt melts are in contact, and we suggest that the spherical inclusion model should not be used here. Finally, both the HS middle bound and the hybrid model with an HS lower bound for the combined melt provide acceptable models that are also consistent with the textural observations. The HS middle bound implies only that the basalt melt is interconnected (there is no statement about the geometry of the sulfide melt and matrix), while the hybrid model explicitly allows for isolated sulfide pockets within an interconnected basalt melt. However, the hybrid model also predicts that the bulk conductivity can decrease with increasing basalt melt fraction, and it is counterintuitive that adding more conductive fraction to a rock can decrease the bulk value. Clearly, laboratory measurements are needed in order to resolve this paradox and determine if this result is a modeling artifact.

7. Conclusions

[33] We have shown that measurements of in situ mantle electrical conductivity and petrological constraints from young xenoliths can be used to predict fractions of basalt melt. Many of the standard models derived from laboratory studies are not helpful in predicting bulk conductivity from the mantle's constituents. Two models, both based on the *Hashin and Shtrikman* [1962] formulation, appear to be most successful in predicting the bulk conductivity of multiple conductive melts embedded in a resistive matrix. These models suggest that <1% basalt melt is permissible in the presence of sulfide melts beneath the modern Sierra Nevada. Only one of these models, the hybrid model, attempts to explicitly include the textural relationship between the basalt and sulfide melts, however. Further

refinement of the modeling will likely require numerical techniques such as random network modeling [*Madden*, 1976] or renormalization group theory [*Madden*, 1983] to more accurately portray the relationship between the basalt melt, the sulfide melt, and matrix. Finally, laboratory measurements are needed to confirm the model predictions presented here.

Appendix A

[34] The derivation for the equation for the equivalent conductivity of a composite sphere follows exactly what *Hashin and Shtrikman* [1962] and *Waff* [1974], except that it includes a middle shell (Figure 9). The derivation is based on the assumption that the composite sphere is replaced by a homogeneous one with a conductivity such that the electrostatic energy is unchanged by the replacement. This process involves equating the potential at the surface of the composite sphere with three layers in a uniform E field to that of a homogeneous sphere with equivalent conductivity, σ_{eff}. If the two potentials are equal, then the composite can be replaced by the homogeneous sphere. The spherical model (Figure 9) in a homogeneous electric field, $\mathbf{E}_0$, is azimuthally symmetric with a z axis aligned along the direction of the field. With this coordinate system, the potential is given by $-E_0 z$. In spherical coordinates, this potential is $\varphi = -E_0 r \cos(\theta)$. Because the external potential on the sphere has only a $\cos(\theta)$ angular dependence, symmetry arguments show that the potential can have only spherical harmonics which involve the Legendre polynomials $P_1^0 = \cos(\theta)$. This means that the general radial dependence for the potential is given by

$$\phi_i = A_i r + \frac{B_i}{r^2}, \tag{A1}$$

where A_i and B_i are coefficients within the ith shell. In order to avoid singularities at the origin ($r = 0$), the potentials in the shells in Figure 9 are

$$\phi_1 = A_1 r, \tag{A2}$$

for the inner shell ($0 \le r \le r_1$),

$$\phi_2 = A_2 r + \frac{B_2}{r^2}, \tag{A3}$$

for the middle shell ($r_1 \le r \le r_2$), and

$$\phi_3 = A_3 r + \frac{B_3}{r^2}. \tag{A4}$$

for the outer shell ($r_2 \le r \le r_3$). Note that the $\cos(\theta)$ dependency has already been factored out of each term in (A2)–(A4). The boundary condition that the potentials be continuous at $r = r_1$, $r = r_2$, and $r = r_3$ leads to the following equalities:

$$A_1 r_1 = A_2 r_1 + \frac{B_2}{r_1^2}, \tag{A5}$$

$$A_3 r_3 + \frac{B_3}{r_3^2} = -E_0 r_3. \tag{A6}$$

Continuity of normal current density across the interfaces, given by

$$J \bullet \hat{r} = \sigma_i \frac{\partial \phi_i}{\partial r} \tag{A7}$$

establishes another set of equalities

$$\sigma_1 A_1 = \sigma_2 \left(A_2 - \frac{2B_2}{r_1^3} \right), \tag{A8}$$

$$\sigma_2 \left(A_2 - \frac{2B_2}{r_2^3} \right) = \sigma_3 \left(A_3 - \frac{2B_3}{r_2^3} \right), \tag{A9}$$

$$\sigma_3 \left(A_3 - \frac{2B_3}{r_3^3} \right) = -\sigma_{eff} E_0. \tag{A10}$$

This last step to equation (A10) actually involves recognizing that the current flowing out of the homogeneous equivalent sphere is equal to that flowing out of the composite sphere and equating the two. (Technically, the left side of equation (A10) is equal to $-\sigma_{\text{outside}} E_0$ and so is the right side if the composite sphere is replaced by an equivalent homogeneous sphere.)

[35] The set of equations (A5)–(A10) provides a unique solution for A_1, A_2, A_3, B_2, B_3, E_0, and σ_{eff}, but we are interested in only the last term. A matrix can be set up and solved for these coefficients as *Waff* [1974] did, but it is cumbersome to set the determinant of that matrix to zero and derive an expression for σ_{eff}. Instead, equations (A8)–(A9) can be expressed in terms of ratios of conductivities

$$A_1 = S_2 \left(A_2 - \frac{2B_2}{r_1^3} \right), \tag{A11}$$

$$A_2 - \frac{2B_2}{r_2^3} = S_3 \left(A_3 - \frac{B_3}{r_2^3} \right), \tag{A12}$$

$$S^* \left(A_3 - \frac{2B_3}{r_3^3} \right) = -E_0. \tag{A13}$$

where $S_2 = \sigma_2/\sigma_1$, $S_3 = \sigma_3/\sigma_2$, $S^* = \sigma_3/\sigma_{\text{eff}}$. Equations (A15) and (A11) can be combined to eliminate A_1 and to solve for B_2 in terms of A_2. This result is substituted into (A6) and (A12) and then combined to eliminate A_2, leaving only A_3 and B_3. Equations (A10) and (A13) can be combined to eliminate E_0, leaving two equations for A_3 and B_3:

$$\frac{1}{S^*} = \frac{A_3 - 2B_3 R_3}{A_3 + B_3 R_3}, \tag{A14}$$

$$\frac{A_3 + B_3 R_2}{1 + \alpha} = \frac{S_3 (A_3 - 2B_3 R_3)}{1 - 2\alpha}, \tag{A15}$$

where $R_2 = 1/r_2^3$, $R_3 = 1/r_3^3$, and

$$\alpha = \frac{S_2 - 1}{2S_2 + 1} \bullet \frac{r_1^3}{r_2^3}. \quad \text{(A16)}$$

Equations (A14) and (A15) can be combined to yield σ_{eff} in terms of the conductivities and radii of the shells

$$\sigma_{eff} = \frac{R_2(2\alpha - 1 - 2S_3 - 2S_3\alpha) - 2R_3(1 - 2\alpha - S_3 - S_3\alpha)}{R_2(2\alpha - 1 - 2S_3 - 2S_3\alpha) + R_3(1 - 2\alpha - S_3 - S_3\alpha)}. \quad \text{(A17)}$$

Recognizing that the volume fractions of the shells are given by $f_1 = 4\Pi r_1^3/3$, $f_2 = 4\Pi(r_2^3 - r_1^3)/3$, and $f_3 = 4\Pi(r_3^3 - r_2^3)/3$, equation (A17) can be rewritten to yield equation (12). As long as the relative volumes of the shells are preserved as the medium is constructed of an infinite number of spheres with an infinite range of radii, the fractions f_i are the volume fractions of each component in the rock.

[36] **Acknowledgments.** Support from the National Science Foundation to Park (EAR 0073707) and to Ducea (EAR 0073607) is gratefully acknowledged. We would like to thank John Booker for his discussions that led to this work and Associate Editor Phil Wannamaker and two anonymous reviewers for their thorough comments.

References

Alard, O., W. L. Griffin, J. P. Lorand, S. E. Jackson, and S. Y. O'Reilly, Non-chondritic distribution of the highly siderophile elements in mantle sulfides, *Nature*, *407*, 891–894, 2000.

Constable, S., and A. Duba, Electrical conductivity of olivine, a dunite, and the mantle, *J. Geophys. Res.*, *95*, 6967–6978, 1990.

Constable, S., T. J. Shankland, and A. Duba, The electrical conductivity of an isotropic olivine mantle, *J. Geophys. Res.*, *97*, 3397–3404, 1992.

Dodge, F. C. W., and J. G. Moore, Late Cenozoic volcanic rocks of the southern Sierra Nevada, California: II. Geochemistry: Summary, *Geol. Soc. Am. Bull.*, *92*, 912–914, 1981.

Dromgoole, E. L., and J. D. Pasteris, Interpretation of the sulfide assemblage in a suite of xenoliths from Kilbourne Hole New Mexico, *Spec. Pap. Geol. Soc. Am.*, *215*, 25–46, 1987.

Duba, A. G., S. Heikamp, W. Meurer, G. Nover, and G. Will, Evidence from borehole samples for the role of accessory minerals in lower-crustal conductivity, *Nature*, *367*, 59–61, 1994.

Ducea, M. N., and S. K. Park, Enhanced mantle conductivity from sulfide minerals, southern Sierra Nevada California, *Geophys. Res. Lett.*, *27*, 2405–2408, 2000.

Ducea, M. N., and J. B. Saleeby, Buoyancy sources for a large, unrooted mountain range, the Sierra Nevada, California: Evidence from xenolith thermobarometry, *J. Geophys. Res.*, *101*, 8229–8244, 1996.

Ducea, M., and J. Saleeby, A case for delamination of the deep batholithic crust beneath the Sierra Nevada California, *Int. Geol. Rev.*, *40*, 78–93, 1998.

Farmer, G. L., A. F. Glazner, and C. R. Manley, Did lithospheric delamination trigger late Cenozoic potassic volcanism in the southern Sierra Nevada California, *Geol. Soc. Am. Bull.*, *114*, 754–768, 2002.

Fleet, M. E., and Y. Pan, Fractional crystallization of anhydrous sulfide liquid in the system Fe-Cu-Ni-S, with applications to magmatic sulfide deposits, *Geochim. Cosmochim. Acta*, *58*, 3369–3377, 1994.

Gaetani, G. A., and T. L. Grove, Wetting of mantle olivine by sulfide melt; Implications for Re/Os ratios in mantle peridotite and late stage core formation, *Earth. Planet. Sci. Lett.*, *169*, 147–163, 1999.

Ghiorso, M. S., and R. O. Sack, Chemical mass transfer in magmatic processes. IV. A revised and internally consistent thermodynamic model for the interpolation and extrapolation of liquid-solid equilibria in magmatic system at elevated temperatures and pressures, *Contrib. Mineral. Petrol.*, *119*, 197–212, 1995.

Guo, J., W. L. Griffin, and S. Y. O'Reilly, Geochemistry and origin of sulfide minerals in mantle xenoliths, Qilin, southeastern China, *J. Petrol.*, *40*, 1125–1149, 1999.

Halliday, D., R. Resnick, and J. Walker, *Fundamentals of Physics*, 1142 pp., John Wiley, New York, 1997.

Handler, M. R., and V. C. Bennett, Behavior of platinum-group elements in the subcontinental mantle of eastern Australia during variable metasomatism and melt depletion, *Geochim. Cosmochim. Acta*, *63*, 3597–3616, 1999.

Hashin, Z., and S. Shtrikman, A variational approach to the theory of effective magnetic permeability of multiphase materials, *J. Appl. Phys.*, *33*, 3125–3131, 1962.

Holzheid, A., M. D. Schmitz, and T. L. Grove, Textural equilibria of iron sulfide liquids in partially molten silicate aggregates and their relevance to core formation scenarios, *J. Geophys. Res.*, *105*, 13,555–13,567, 2000.

Jones, C. H., H. Kanamori, and S. W. Roecker, Missing roots and mantle "drips": Regional *Pn* and teleseismic arrival times in the southern Sierra Nevada and vicinity California, *J. Geophys. Res.*, *99*, 4567–4601, 1994.

Kaiura, G. H., and J. M. Toguri, Densities of molten FeS, FeS-Cu_2S and Fe-S-0 system-utilizing a bottom-balance Archimedean technique, *Can. Metall. Q.*, *18*, 155–164, 1979.

Keays, R. R., The role of komatiitic and picritic magmatism and S-saturation in the formation of ore deposits, *Lithos*, *34*, 1–18, 1995.

Lee, C. T., Q. Yin, R. L. Rudnick, J. T. Chesley, and S. B. Jacobsen, Osmium isotopic evidence for Mesozoic removal of lithospheric mantle beneath the Sierra Nevada, California, *Science*, *289*, 1912–1916, 2000.

Lee, C. T., R. L. Rudnick, and G. Brimhall Jr., Deep lithospheric dynamics beneath the Sierra Nevada during the Mesozoic and Cenozoic as inferred from xenolith petrology, *Geochem. Geophys. and Geosystems*, *2*, 10.1029/2001GC000152, 2001.

Lorand, J. P., Abundance and distribution of Cu-Fe-Ni sulfides, sulfur, copper and platinum group elements in orogenic-type spinel lherzolite massifs of Ariege (northeastern Pyrenees, France), *Earth Planet. Sci. Lett.*, *93*, 50–64, 1989.

Lorand, J. P., Are spinel lherzolite xenoliths representative of the sulfur content of the upper mantle?, *Geochim. Cosmochim. Acta*, *54*, 1487–1492, 1990.

Lorand, J. P., and F. Conquere, Contribution l'etude des sulfures dans les enclaves de lherzolite a spinelle des basaltes alcalins, *Bull. Mineral.*, *106*, 585–606, 1983.

Madden, T. R., Random networks and mixing laws, *Geophysics*, *41*, 1104–1125, 1976.

Madden, T. R., Microcrack connectivity in rocks: A renormalization group approach to the critical phenomena of conductivity and failure in crystalline rocks, *J. Geophys. Res.*, *88*, 585–592, 1983.

Mareschal, M., R. L. Kellett, R. D. Kurtz, J. N. Ludden, and R. C. Bailey, Archean cratonic roots, mantle shear zones, and deep electrical conductivity, *Nature*, *375*, 134–137, 1995.

Mavrogenes, J. A., and H. S. T. O'Neill, The relative effects of pressure, temperature and oxygen fugacity on the solubility of sulfide in mafic magmas, *Geochim. Cosmochim. Acta*, *63*, 1173–1180, 1999.

Minarek, W. G., F. J. Ryerson, and E. B. Watson, Textural entrapment of core-forming melts, *Science*, *272*, 530–532, 1996.

Moore, J. G., and F. C. Dodge, Late Cenozoic volcanic rocks of the southern Sierra Nevada, California; I. Geology and petrology, *Geol. Soc. Am. Bull.*, *91*, 515–518, 1980.

Naldrett, A. J., *Magmatic Sulfide Deposits*, Clarendon, Oxford, UK, 1989.

Olhoeft, G. R., Electrical conductivity, in *Physical Properties of Rocks and Minerals*, edited by N. S. Touloukian, W. R. Judd, and R. F. Roy, pp. 257–328, McGraw-Hill, New York, 1981.

Park, S. K., B. Hirasuna, G. R. Jiracek, and C. L. Kinn, Magnetotelluric evidence of lithospheric mantle thinning beneath the southern Sierra Nevada, *J. Geophys. Res.*, *101*, 16,241–16,255, 1996.

Pearson, N. J., O. Alard, W. L. Griffin, S. E. Jackson, and S. Y. O'Reilly, In-situ measurement of Re-Os isotopes in mantle sulfides by laser-ablation multicollector-inductively coupled plasma mass spectrometry: Analytical methods and preliminary results, *Geochim. Cosmochim. Acta*, *66*, 1037–1050, 2002.

Roberts, J. J., and J. A. Tyburczy, Partial-melt electrical conductivity: Influences of melt composition, *J. Geophys. Res.*, *104*, 7055–7065, 1999.

Ruppert, S., M. M. Fliedner, and G. Zandt, Thin crust and active upper mantle beneath the southern Sierra Nevada in the western United States, *Tectonophysics*, *286*, 237–252, 1998.

Ryzenkho, B., and G. Kennedy, The effect of pressure on the eutectic in the Fe-FeS system, *Am. J. Sci.*, *273*, 800–810, 1973.

Shankland, T. J., and H. S. Waff, Partial melting and electrical conductivity anomalies in the upper mantle, *J. Geophys. Res.*, *82*, 5409–5417, 1977.

Shaw, C. S. J., Origin of sulfide blebs in variably metasomatized mantle xenoliths, quaternary West Eifel volcanic field, Germany, *Can. Mineral.*, *35*, 1453–1463, 1997.

Smith, D., Insights into the evolution of the uppermost continental mantle from xenolith localities on and near the Colorado Plateau and regional comparisons, *J. Geophys. Res.*, *105*, 16,769–16,781, 2000.

Snow, J. K., and B. Wernicke, Cenozoic tectonism in the central Basin and Range: Magnitude, rate, and distribution of upper crustal strain, *Am. J. Sci.*, *300*, 659–719, 1998.

Szabo, C., and R. J. Bodnar, Chemistry and origin of mantle sulfides in spinel peridotite xenoliths from alkaline basaltic lavas, Nograd-Gomor Volcanic field, *Geochim. Cosmochim. Acta*, *59*, 3917–3972, 1995.

Tyburczy, J. A., and H. S. Waff, Electrical conductivity of molten basalt and andesite to 20 kbar pressure: Geophysical significance and implications for charge transport and melt structure, *J. Geophys. Res.*, *88*, 2413–2430, 1983.

Vozoff, K., The magnetotelluric method, in *Electromagnetic Methods in Applied Geophysics*, edited by M. N. Nabighian, pp. 641–711, Soc. of Explor. Geophys., Tulsa, Okla., 1991.

Waff, H. S., Theoretical considerations of electrical conductivity in a partially molten mantle and implications for geothermometry, *J. Geophys. Res.*, *79*, 4003–4010, 1974.

Wernicke, B., et al., Origin of high mountains in the continents: The southern Sierra Nevada, *Science*, *271*, 190–193, 1996.

Wilson, M. R., T. K. Kyser, and R. Fagan, Sulfur isotope systematics and platinum-group element behavior in REE-enriched metasomatic fluids: A study of mantle xenoliths from Dish Hill, California, USA, *Geochim. Cosmochim. Acta*, *11*, 1933–1942, 1996.

Xu, Y., T. J. Shankland, and B. T. Poe, Laboratory-based electrical conductivity in the Earth's mantle, *J. Geophys. Res.*, *105*, 27,865–27,875, 2000.

M. N. Ducea, Department of Geological Sciences, University of Arizona, Tucson, AZ 85711, USA.

S. K. Park, Institute of Geophysics and Planetary Physics, University of California, 1432 Geology, Riverside, CA 92521-0412, USA. (magneto@ucrmt.ucr.edu)